VII International Conference on Computational Methods for Coupled Problems in Science and Engineering
COUPLED PROBLEMS 2017
M. Papadrakakis, E. Oñate and B. Schrefler (Eds)

A THERMO-HYDRO-MECHANICAL FINITE ELEMENT MODEL OF FREEZING IN POROUS MEDIA—THERMO-MECHANICALLY CONSISTENT FORMULATION AND APPLICATION TO GROUND SOURCE HEAT PUMPS

Tianyuan Zheng[*†], Xing-Yuan Miao[*†], Dmitri Naumov[*†], Haibing Shao[*#], Olaf Kolditz[*†] and Thomas Nagel[*‡]

[*]Department of Environmental Informatics, Helmholtz Centre for Environmental Research – UFZ
Permoserstr. 15, 04318 Leipzig, Germany
e-mail: tianyuan.zheng@ufz.de, web page: http://www.ufz.com/

[†]Applied Environmental Systems Analysis, Technische Universität Dresden
01069 Dresden, Germany
web page: http://tu-dresden.de/

#Faculty of Geoscience, Geoengineering and Mining, Freiberg University of Mining and Technology
Akademiestraße 6, 09599 Freiberg
web page: http://tu-freiberg.de/

[‡]Department of Mechanical and Manuf. Engineering, School of Engineering, Trinity College Dublin
College Green, Dublin 2, Ireland
web page: http://www.tcd.ie/

Key words: freezing and thawing, phase change, Theory of Porous Media, geothermal energy, borehole heat exchanger, OpenGeoSys

Abstract. Freezing phenomena in porous media have attracted great attention in geotechnics, construction engineering and geothermal energy. For shallow geothermal applications where heat pumps are connected to borehole heat exchangers (BHEs), soil freezing around the BHEs is a potential problem due to persistent heat extraction or inappropriate design which can significantly influence the temperature distribution as well as groundwater flow patterns in the subsurface, and even lead to frost heave. A fully coupled thermo-hydro-mechanical freezing model is required for advanced system design and scenario analyses. In the framework of the Theory of Porous Media, a triphasic freezing model is derived and solved with the finite element method. Ice formation in the porous medium results from a coupled heat and mass transfer problem with phase change and is accompanied by volume expansion. The model is able to capture various coupled physical phenomena during freezing, e.g., the latent heat effect, groundwater flow with porosity change and mechanical deformation. The current paper is focused primarily on the theoretical derivation of the conceptual model. Its numerical imple-

mentation is verified against analytical solutions of selected phenomena including pure phase change and thermo-hydro-mechanical process couplings.

1 Introduction

Among different coupled processes, the thermal-hydro-mechanical behaviour of solid-liquid phase change in general and freezing in fluid-saturated porous media in particular is of great interest in soil construction [1], geotechnics [2], energy storage [3] and geothermal applications [4, 5]. Considering shallow geothermal energy, ground source heat pump systems (GSHPS) are increasingly employed as an efficient technology for the heating and cooling of buildings. The general proposition of a GSHPS is to extract heat from the shallow subsurface (50 m – 200 m below the surface) by circulating a heat-transfer fluid through single or multiple borehole heat exchangers (BHE). The energy carried by the circulating fluid is then lifted by heat pumps to temperature levels suitable for domestic applications. In cold regions, the undisturbed soil temperature is already below 10 °C [6]. When its temperature drops below 0 °C due to continuous heat extraction or inappropriate BHE/GSHPS design, freezing of the groundwater surrounding the BHEs will occur [7]. This will not only strongly affect the soil temperature distribution, hydraulic properties and the heat pump efficiency but may also cause mechanical damage to the BHEs and the surrounding facilities [4, 8]. For a discussion of implications on the design length of BHEs and economic aspects, cf. Zheng et al. [5].

In order to quantitatively analyze these coupled multi-physical phenomena on an engineering scale, a reliable macroscopic, fully coupled thermo-hydro-mechanical model is required which captures the relevant phenomena. The macroscopic Theory of Porous Media (TPM) [9, 10, 11] has been selected here as an ideal framework for this task.

A fundamental mathematical model based on mixture theory and thermodynamical principles was established for saturated porous media by [12]. Another macroscopic ternary model [13] incorporating liquid, ice and solid was constructed based on the theory of poromechanics by Coussy. As an extension of this model [13], Zhou & Meschke [2] developed a ternary model in view of a detailed physical description of ice crystallization. In recent years, the Theory of Porous Media was employed and Bluhm et al. [10, 14] presented a ternary model derived from thermodynamical considerations. Later Lai et al. [18] proposed a theoretical model of thermo-hydro-mechanical interactions during freezing and validated it with experiments. For the unsaturated cases, Li et al. [15, 16] demonstrated the heat-moisture-deformation coupling based on a theoretical framework with and without explicit consideration of the gas phase. Differing from considering gas as an extra phase, Liu & Yu [17] directly employed Richard's equation to capture the fluid flow in the unsaturated zone.

In the present paper, a fully coupled thermo-mechanically consistent THM freezing model for liquid-saturated porous materials is derived based on the Theory of Porous Media by exploiting the entropy inequality. In contrast to some of the previous models, Truesdell's metaphysical principles [19] are strictly adhered to for the mixture balance relations. The description of the

mechanical behaviour of the ice and solid phases accounts for their differing natural configurations.

The fundamental kinematics and balance relations are listed in Section 2. The assumptions made and constitutive relations derived from the Clausius-Duhem inequality are presented in Section 3. With the balance relations and constitutive laws, the governing equations are given in Section 4. The verification of the numerical model is performed in Section 5. The paper closes with an illustrative numerical example in Section 6.

2 General definitions

2.1 Kinematics

Consider a medium composed of different phases or constituents α, each represented by a substitute continuum defined on the entire control space. The motion of a constituent α is described by its motion function $\boldsymbol{\chi}_\alpha$ that maps the position $\mathbf{X}_\alpha$ of a material point (particle) in the reference configuration to its spatial location $\mathbf{x}$ in the current configuration:

$$\mathbf{x} = \boldsymbol{\chi}_\alpha(\mathbf{X}_\alpha, t) \tag{1}$$

Each phase can then be assigned a deformation gradient as well as its inverse

$$\mathbf{F}_\alpha = \mathrm{Grad}_\alpha\, \mathbf{x} \quad \text{and} \quad \mathbf{F}_\alpha^{-1} = \mathrm{grad}\, \mathbf{X}_\alpha \tag{2}$$

and the material time derivative following the motion of a phase α defines the phase velocities

$$\mathbf{v}_\alpha = \mathbf{x}'_\alpha = \frac{\partial \boldsymbol{\chi}_\alpha(\mathbf{X}_\alpha, t)}{\partial t} \tag{3}$$

Based on these fundamental kinematic definitions, the entire spectrum of continuum mechanical kinematic quantities becomes available, e.g. the material and spatial velocity gradients:

$$(\mathbf{F}_\alpha)'_\alpha = \mathrm{Grad}_\alpha\, \mathbf{x}'_\alpha \quad \text{and} \quad \mathbf{l}_\alpha = \mathrm{grad}\, \mathbf{x}'_\alpha = (\mathbf{F}_\alpha)'_\alpha\, \mathbf{F}_\alpha^{-1} \tag{4}$$

Following the above relations, the right Cauchy-Green deformation tensor and Green-Lagrangean strain tensor read:

$$\mathbf{C}_\alpha = \mathbf{F}_\alpha^T \mathbf{F}_\alpha \quad \text{and} \quad \mathbf{E}_\alpha = \frac{1}{2}(\mathbf{C}_\alpha - \mathbf{I}) \tag{5}$$

When small-strain conditions are assumed, the finite deformation approach can be reduced to a geometrically linear one via $\mathrm{lin}\, \mathbf{E}_\alpha = \boldsymbol{\epsilon}_\alpha$ and the distinction between reference configuration and current configuration is no longer necessary in the spatial operators. For further definitions, see standard texts on continuum mechanics [19].

Based on Truesdell's metaphysical principles [19], the motion of the mixture is governed by the same equations as the motion of a single body. Hence, summation of the balance equations of the individual phases listed in the subsequent section must yield the balance equations known from continuum mechanics of single phase materials. This condition imposes restrictions on the production terms. For details, the reader is referred to, e.g., [9] and references therein.

3 Balance equations and constitutive relations

3.1 Specific assumptions

To maintain a certain level of generality in the conceptual modelling section, a finite strain setting will be maintained throughout the derivation of the model. A first implementation of the governing equations will then rest on the assumption of linear kinematics.

Before specifying the balance equations, some basic assumptions of the model shall be clarified.

1. A three-phase mixture consisting of solid (S), ice (I) and the aqueous pore fluid (L) is considered: $\alpha = \{\mathrm{S}, \mathrm{I}, \mathrm{L}\}$.
2. For all phases we assume incompressibility in the sense $\varrho_{\alpha\mathrm{R}} = \varrho_{\alpha\mathrm{R}}(T)$.
3. Deformation and flow occur in a quasi-static fashion such that inertial effects can be neglected in the final governing equations: $\mathbf{a}_\alpha = \mathbf{0}$.
4. The local temperatures of all constituents are equal (local thermal equilibrium): $T_\alpha = T$.
5. Mass transfer is limited to the water and ice phases, i.e. $\hat{\varrho}_\mathrm{S} = 0$, $\hat{\varrho}_\mathrm{L} = -\hat{\varrho}_\mathrm{I}$.
6. The constituents solid and ice are kinematically constrained once the ice is formed at time t_F, i.e. $\mathbf{v}_\mathrm{S} = \mathbf{v}_\mathrm{I}$. At that stage, the solid may have undergone a motion already, i.e. the reference coordinates of an ice particle are given by $\widehat{\mathbf{X}}_\mathrm{I} = \chi_\mathrm{S}(\mathbf{X}_\mathrm{S}, t_\mathrm{F})$. The current placement of corresponding solid and ice particles is then given by the motion function of ice and solid via $\mathbf{x} = \chi_\mathrm{S}(\mathbf{X}_\mathrm{S}, t) = \chi_\mathrm{I}(\widehat{\mathbf{X}}_\mathrm{I}, t) = \chi_\mathrm{I}\left(\chi_\mathrm{S}(\mathbf{X}_\mathrm{S}, t_\mathrm{F}), t\right)$.

Assumption 6 will be captured by a multiplicative decomposition of the deformation gradient of the solid into a part before freezing (S0) and a part after freezing (I) following [10]

$$\mathbf{F}_\mathrm{S} = \widehat{\mathbf{F}}_\mathrm{I}\mathbf{F}_\mathrm{S0} \tag{6}$$

It will be assumed that stresses in the ice are only determined by that part of the motion accrued after freezing has occurred, i.e. by $\widehat{\mathbf{F}}_\mathrm{I}$, while the stress response of the solid is characterised by $\mathbf{F}_\mathrm{S}$ itself. Under the small-strain assumption, the decomposition of the motion simplifies to:

$$\boldsymbol{\epsilon}_\mathrm{S} = \boldsymbol{\epsilon}_\mathrm{I} + \boldsymbol{\epsilon}_\mathrm{S0} \tag{7}$$

Based on the general mass balance in the form

$$\phi_\alpha(\varrho_{\alpha\mathrm{R}})'_\alpha + (\phi_\alpha)'_\alpha\varrho_{\alpha\mathrm{R}} + \varrho_{\alpha\mathrm{R}}\phi_\alpha \operatorname{div}\mathbf{v}_\alpha = \hat{\varrho}_\alpha \tag{8}$$

as well Assumptions 5 and 6, the derivatives of the individual volume fractions are obtained from the above mass balances in the following form

$$(\phi_{\mathrm{S}})'_{\mathrm{S}} = -\phi_{\mathrm{S}}\mathrm{div}\mathbf{v}_{\mathrm{S}} - \phi_{\mathrm{S}}\frac{(\varrho_{\mathrm{SR}})'_{\mathrm{S}}}{\varrho_{\mathrm{SR}}} \tag{9}$$

$$(\phi_{\mathrm{I}})'_{\mathrm{S}} = \frac{\hat{\varrho}_{\mathrm{I}}}{\varrho_{\mathrm{IR}}} - \phi_{\mathrm{I}}\mathrm{div}\mathbf{v}_{\mathrm{S}} - \phi_{\mathrm{I}}\frac{(\varrho_{\mathrm{IR}})'_{\mathrm{S}}}{\varrho_{\mathrm{IR}}} \tag{10}$$

$$(\phi_{\mathrm{L}})'_{\mathrm{S}} = -\frac{\hat{\varrho}_{\mathrm{I}}}{\varrho_{\mathrm{LR}}} - \phi_{\mathrm{L}}\mathrm{div}\mathbf{v}_{\mathrm{L}} - \phi_{\mathrm{L}}\frac{(\varrho_{\mathrm{LR}})'_{\mathrm{L}}}{\varrho_{\mathrm{LR}}} - \mathrm{grad}\phi_{\mathrm{L}} \cdot \mathbf{w}_{\mathrm{LS}} \tag{11}$$

Based on Assumption 2, the time derivative of the material density can be expressed via the temperature rate and the volumetric thermal expansion coefficient $\beta_{T\alpha}$

$$(\varrho_{\alpha\mathrm{R}})'_{\alpha} = \frac{\partial \varrho_{\alpha\mathrm{R}}}{\partial T}T'_{\alpha} = -\varrho_{\alpha\mathrm{R}}\beta_{T\alpha}T'_{\alpha} \quad \text{with} \quad \beta_{T\alpha} = -\frac{1}{\varrho_{\alpha\mathrm{R}}}\frac{\partial \varrho_{\alpha\mathrm{R}}}{\partial T} \tag{12}$$

3.2 Saturation condition

The saturation condition for this ternary mixture can be written in absolute and in rate form (following the trajectory of the solid) as

$$\sum_{\alpha}\phi_{\alpha} = 1 \quad \text{and} \quad \sum_{\alpha}(\phi_{\alpha})'_{\mathrm{S}} = 0 \tag{13}$$

Substitution of Eqs. (9)–(11) yields the model-specific form of the mixture volume balance:

$$0 = \mathrm{div}\left[\mathbf{v}_{\mathrm{S}} + \phi_{\mathrm{L}}\mathbf{w}_{\mathrm{LS}}\right] + \hat{\varrho}_{\mathrm{I}}\left(\varrho_{\mathrm{LR}}^{-1} - \varrho_{\mathrm{IR}}^{-1}\right) + \frac{\phi_{\mathrm{S}}(\varrho_{\mathrm{SR}})'_{\mathrm{S}}}{\varrho_{\mathrm{SR}}} + \frac{\phi_{\mathrm{I}}(\varrho_{\mathrm{IR}})'_{\mathrm{S}}}{\varrho_{\mathrm{IR}}} + \frac{\phi_{\mathrm{L}}(\varrho_{\mathrm{LR}})'_{\mathrm{L}}}{\varrho_{\mathrm{LR}}} \tag{14}$$

3.3 Evaluation of the entropy inequality

The entropy inequality will be exploited following the Coleman-Noll procedure. Invoking the assumption of local thermal equilibrium, the production-term constraint in the energy balance, and adding the saturation condition as a constraint to the entropy inequality yields

$$\begin{aligned} 0 \leq \sum_{\alpha=1}^{\kappa}\Bigg\{ & -\varrho_{\alpha}[(\psi_{\alpha})'_{\alpha} + T'_{\alpha}\eta_{\alpha}] - \hat{\varrho}_{\alpha}\left(\psi_{\alpha} - \frac{1}{2}\mathbf{v}_{\alpha}\cdot\mathbf{v}_{\alpha}\right) + \\ & \boldsymbol{\sigma}_{\alpha} : \mathbf{l}_{\alpha} - \hat{\mathbf{p}}_{\alpha}\cdot\mathbf{v}_{\alpha} - \frac{1}{T}\mathbf{q}_{\alpha}\cdot\mathrm{grad}\,T - \lambda(\phi_{\alpha})'_{\mathrm{S}}\Bigg\} \end{aligned} \tag{15}$$

The Lagrange multiplier λ can be understood as a pressure-type reaction force enforcing the saturation constraint.

Employing the principle of phase-separation [9], the free energy of the solid phase is assumed to depend on solid deformation and temperature, the liquid phase free energy only on temperature, and the free energy of the ice phase on the ice volume fraction, temperature and that part of the deformation characterizing ice deformation, cf. Eq. 6. Hence, the following *Ansatz* is made for the specific Helmholtz free energies:

$$\psi_{\mathrm{S}} = \psi_{\mathrm{S}}(\mathbf{C}_{\mathrm{S}}, T) \qquad \psi_{\mathrm{I}} = \psi_{\mathrm{I}}(\widehat{\mathbf{C}}_{\mathrm{I}}, T, \phi_{\mathrm{I}}) \qquad \psi_{\mathrm{L}} = \psi_{\mathrm{L}}(T) \tag{16}$$

where the right Cauchy-Green tensors $\mathbf{C}_{\mathrm{S}} = \mathbf{F}_{\mathrm{S}}^{\mathrm{T}}\mathbf{F}_{\mathrm{S}}$ and $\widehat{\mathbf{C}}_{\mathrm{I}} = \widehat{\mathbf{F}}_{\mathrm{I}}^{\mathrm{T}}\widehat{\mathbf{F}}_{\mathrm{I}}$ have been used.

Neglecting terms associated with the kinetic energy of mass transfer, and using the transformed mass balance equations (9)–(11), inequality (15) can be expanded to

$$\begin{aligned} 0 \leq\ & -\varrho_{\mathrm{S}}(\psi_{\mathrm{S}})'_{\mathrm{S}} + T'_{\mathrm{S}}\left(-\varrho_{\mathrm{S}}\eta_{\mathrm{S}} + \lambda\frac{\phi_{\mathrm{S}}}{\varrho_{\mathrm{SR}}}\frac{\partial\varrho_{\mathrm{SR}}}{\partial T}\right) - \varrho_{\mathrm{I}}(\psi_{\mathrm{I}})'_{\mathrm{S}} + T'_{\mathrm{S}}\left(-\varrho_{\mathrm{I}}\eta_{\mathrm{I}} + \lambda\frac{\phi_{\mathrm{I}}}{\varrho_{\mathrm{IR}}}\frac{\partial\varrho_{\mathrm{IR}}}{\partial T}\right) - \\ & - \varrho_{\mathrm{L}}(\psi_{\mathrm{L}})'_{\mathrm{L}} + T'_{\mathrm{L}}\left(-\varrho_{\mathrm{L}}\eta_{\mathrm{L}} + \lambda\frac{\phi_{\mathrm{L}}}{\varrho_{\mathrm{LR}}}\frac{\partial\varrho_{\mathrm{LR}}}{\partial T}\right) - \hat{\varrho}_{\mathrm{I}}\left(\psi_{\mathrm{I}} + \frac{\lambda}{\varrho_{\mathrm{IR}}} - \psi_{\mathrm{L}} - \frac{\lambda}{\varrho_{\mathrm{LR}}}\right) + \\ & + (\boldsymbol{\sigma}_{\mathrm{S}} + \lambda\phi_{\mathrm{S}}\mathbf{I}) : \mathbf{d}_{\mathrm{S}} + (\boldsymbol{\sigma}_{\mathrm{I}} + \lambda\phi_{\mathrm{I}}\mathbf{I}) : \mathbf{d}_{\mathrm{S}} + (\boldsymbol{\sigma}_{\mathrm{L}} + \lambda\phi_{\mathrm{L}}\mathbf{I}) : \mathbf{d}_{\mathrm{L}} - \\ & - \sum_{\alpha}\hat{\mathbf{p}}_{\alpha}\cdot\mathbf{v}_{\alpha} + \lambda\,\mathrm{grad}\,\phi_{\mathrm{L}}\cdot\mathbf{w}_{\mathrm{LS}} - \frac{1}{T}\mathbf{q}_{\mathrm{SIL}}\cdot\mathrm{grad}\,T \quad \text{with} \quad \mathbf{q}_{\mathrm{SIL}} = \sum_{\alpha}\mathbf{q}_{\alpha} \end{aligned} \tag{17}$$

Now, the terms $\boldsymbol{\sigma}_{\alpha}^{\mathrm{E}} = \boldsymbol{\sigma}_{\alpha} + \lambda\phi_{\alpha}\mathbf{I}$ defining the so-called extra stresses can be introduced. Based on dimensional analyses, it is common practice to neglect fluid extra stresses. Hence, we find a hydrostatic stress state in the fluid and identify the Lagrange multiplier λ with the pore pressure p_{LR}:

$$\boldsymbol{\sigma}_{\mathrm{L}} = -p_{\mathrm{LR}}\phi_{\mathrm{L}}\mathbf{I} \quad \text{with} \quad \lambda = p_{\mathrm{LR}} \tag{18}$$

The constraint on the momentum production terms yields the relation

$$-(\hat{\mathbf{p}}_{\mathrm{S}} + \hat{\mathbf{p}}_{\mathrm{I}}) = \hat{\mathbf{p}}_{\mathrm{L}} + \hat{\varrho}_{\mathrm{I}}\mathbf{w}_{\mathrm{LS}} \tag{19}$$

Similarly to the stresses, the extra momentum production is the constitutively determined term in addition to effects contributed by the Lagrange multiplier—i.e. the liquid pressure—and is defined as

$$\hat{\mathbf{p}}_{\mathrm{L}}^{\mathrm{E}} = \hat{\mathbf{p}}_{\mathrm{L}} - \lambda\,\mathrm{grad}\,\phi_{\mathrm{L}} \tag{20}$$

With Eq. (16) and $(\mathbf{C}_{\alpha})'_{\alpha} = 2\mathbf{F}_{\alpha}^{\mathrm{T}}\mathbf{d}_{\alpha}\mathbf{F}_{\alpha}$ we can now write

$$\begin{aligned} 0 \leq\ & \left(\boldsymbol{\sigma}_{\mathrm{S}}^{\mathrm{E}} - 2\varrho_{\mathrm{S}}\mathbf{F}_{\mathrm{S}}\frac{\partial\psi_{\mathrm{S}}}{\partial\mathbf{C}_{\mathrm{S}}}\mathbf{F}_{\mathrm{S}}^{\mathrm{T}}\right) : \mathbf{d}_{\mathrm{S}} + \left(\boldsymbol{\sigma}_{\mathrm{I}}^{\mathrm{E}} - 2\varrho_{\mathrm{I}}\hat{\mathbf{F}}_{\mathrm{I}}\frac{\partial\psi_{\mathrm{I}}}{\partial\hat{\mathbf{C}}_{\mathrm{I}}}\hat{\mathbf{F}}_{\mathrm{I}}^{\mathrm{T}} + \varrho_{\mathrm{I}}\phi_{\mathrm{I}}\frac{\partial\psi_{\mathrm{I}}}{\partial\phi_{\mathrm{I}}}\mathbf{I}\right) : \mathbf{d}_{\mathrm{S}} - \\ & - \sum_{\alpha}\varrho_{\alpha}\left(\eta_{\alpha} - \lambda\frac{1}{(\varrho_{\alpha\mathrm{R}})^2}\frac{\partial\varrho_{\alpha\mathrm{R}}}{\partial T} + \frac{\partial\psi_{\alpha}}{\partial T}\right)T'_{\alpha} - \hat{\varrho}_{\mathrm{I}}\left[\psi_{\mathrm{I}} + \frac{1}{\varrho_{\mathrm{IR}}}\left(\lambda + \phi_{\mathrm{I}}\frac{\partial\psi_{\mathrm{I}}}{\partial\phi_{\mathrm{I}}}\right) - \psi_{\mathrm{L}} - \frac{\lambda}{\varrho_{\mathrm{LR}}}\right] - \\ & - \varrho_{\mathrm{I}}\phi_{\mathrm{I}}\beta_{T\mathrm{I}}\frac{\partial\psi_{\mathrm{I}}}{\partial\phi_{\mathrm{I}}}T'_{\mathrm{S}} - \hat{\mathbf{p}}_{\mathrm{L}}^{\mathrm{E}}\cdot\mathbf{w}_{\mathrm{LS}} - \frac{1}{T}\mathbf{q}_{\mathrm{SIL}}\cdot\mathrm{grad}\,T \end{aligned} \tag{21}$$

This form motivates the introduction of the extra entropy terms $\eta_{\alpha}^{\mathrm{E}}$ such that

$$\eta_\alpha = \eta_\alpha^{\mathrm{E}} + \lambda \frac{1}{(\varrho_{\alpha\mathrm{R}})^2} \frac{\partial \varrho_{\alpha\mathrm{R}}}{\partial T} = \eta_\alpha^{\mathrm{E}} - \frac{\beta_{T\alpha}}{\varrho_{\alpha\mathrm{R}}} p_{\mathrm{LR}} \tag{22}$$

Based on the *Ansatz* defined in Eq. (16), the following restrictions can be derived:

$$\eta_\alpha^{\mathrm{E}} = -\frac{\partial \psi_\alpha}{\partial T} \quad \text{and} \quad \eta_\alpha = \eta_\alpha^{\mathrm{E}} - \frac{\beta_{T\alpha}}{\varrho_{\alpha\mathrm{R}}} p_{\mathrm{LR}} \quad \text{for } \alpha = \mathrm{S} \text{ and } \mathrm{L} \tag{23}$$

$$\eta_{\mathrm{I}}^{\mathrm{E,F}} = -\frac{\partial \psi_{\mathrm{I}}}{\partial T} \quad \text{and} \quad \eta_{\mathrm{I}} = \eta_{\mathrm{I}}^{\mathrm{E,F}} - \frac{\beta_{T\mathrm{I}}}{\varrho_{\mathrm{IR}}} \underbrace{\left(p_{\mathrm{LR}} + \varrho_{\mathrm{I}} \frac{\partial \psi_{\mathrm{I}}}{\partial \phi_{\mathrm{I}}} \right)}_{p_{\mathrm{red}}} \quad \text{with} \quad \eta_{\mathrm{I}}^{\mathrm{E,F}} = \eta_{\mathrm{I}}^{\mathrm{E}} + \frac{\beta_{T\mathrm{I}}}{\varrho_{\mathrm{IR}}} \varrho_{\mathrm{I}} \frac{\partial \psi_{\mathrm{I}}}{\partial \phi_{\mathrm{I}}} \tag{24}$$

$$\boldsymbol{\sigma}_{\mathrm{S}} = -p_{\mathrm{LR}} \phi_{\mathrm{S}} \mathbf{I} + 2 \varrho_{\mathrm{S}} \mathbf{F}_{\mathrm{S}} \frac{\partial \psi_{\mathrm{S}}}{\partial \mathbf{C}_{\mathrm{S}}} \mathbf{F}_{\mathrm{S}}^{\mathrm{T}} \tag{25}$$

$$\boldsymbol{\sigma}_{\mathrm{I}} = -\phi_{\mathrm{I}} \underbrace{\left(p_{\mathrm{LR}} + \varrho_{\mathrm{I}} \frac{\partial \psi_{\mathrm{I}}}{\partial \phi_{\mathrm{I}}} \right)}_{P\mathrm{red}} \mathbf{I} + 2 \varrho_{\mathrm{I}} \hat{\mathbf{F}}_{\mathrm{I}} \frac{\partial \psi_{\mathrm{I}}}{\partial \hat{\mathbf{C}}_{\mathrm{I}}} \hat{\mathbf{F}}_{\mathrm{I}}^{\mathrm{T}} \tag{26}$$

Introducing the chemical potential-type quantities

$$\Psi_{\mathrm{I}} = \psi_{\mathrm{I}} + \frac{p_{\mathrm{red}}}{\varrho_{\mathrm{IR}}} \quad \text{and} \quad \Psi_{\mathrm{L}} = \psi_{\mathrm{L}} + \frac{p_{\mathrm{LR}}}{\varrho_{\mathrm{LR}}} \tag{27}$$

allows the formulation of the remaining dissipation inequality as

$$\mathcal{D} = -\hat{\mathbf{p}}_{\mathrm{L}}^{\mathrm{E}} \cdot \mathbf{w}_{\mathrm{LS}} - \frac{1}{T} \mathbf{q}_{\mathrm{SIL}} \cdot \operatorname{grad} T - \hat{\varrho}_{\mathrm{I}} (\Psi_{\mathrm{I}} - \Psi_{\mathrm{L}}) \geq 0 \tag{28}$$

Treating physically distinct terms independently, the heat flux vector can be found from the linear relation

$$0 \leq -\mathbf{q}_{\mathrm{SIL}} \cdot \operatorname{grad} T \quad \rightarrow \quad \mathbf{q}_{\mathrm{SIL}} = -\boldsymbol{\lambda}_{\mathrm{SIL}} \operatorname{grad} T \quad \text{with} \quad \mathbf{a} \cdot \boldsymbol{\lambda}_{\mathrm{SIL}} \mathbf{a} \geq 0 \; \forall \; \mathbf{a} \neq \mathbf{0} \tag{29}$$

where $\boldsymbol{\lambda}_{\mathrm{SIL}}$ is the effective heat conductivity tensor of the saturated porous medium.
Similarly, the flow-law can be derived from a linear relationship as

$$0 \leq -\hat{\mathbf{p}}_{\mathrm{L}}^{\mathrm{E}} \cdot \mathbf{w}_{\mathrm{LS}} \quad \rightarrow \quad \hat{\mathbf{p}}_{\mathrm{L}}^{\mathrm{E}} = -\mathbf{S}\mathbf{w}_{\mathrm{LS}} \quad \text{with} \quad \mathbf{a} \cdot \mathbf{S}\mathbf{a} \geq 0 \; \forall \; \mathbf{a} \neq \mathbf{0} \tag{30}$$

Substituting the fluid stress tensor from Eq. (18) and the flow law from relation (30) into the fluid momentum balance and choosing $\mathbf{S}^{-1} = \mathbf{K}/(\mu_{\mathrm{LR}} \phi_{\mathrm{L}}^2)$ recovers a Darcy-like law:

$$\phi_{\mathrm{L}} \mathbf{w}_{\mathrm{LS}} = -\frac{\mathbf{K}}{\mu_{\mathrm{LR}}} \left(\operatorname{grad} p_{\mathrm{LR}} - \varrho_{\mathrm{LR}} \mathbf{b}_{\mathrm{L}} \right) \tag{31}$$

In which K is the permeability and varies with the ice formation which occupies the porosity. Finally, a kinetic law for the phase transition can be defined based on the difference in the chemical potentials of the liquid and ice phases:

$$0 \leq -\hat{\varrho}_{\mathrm{I}} (\Psi_{\mathrm{I}} - \Psi_{\mathrm{L}}) \quad \rightarrow \quad \hat{\varrho}_{\mathrm{I}} = c_{\mathrm{F}} (\Psi_{\mathrm{L}} - \Psi_{\mathrm{I}}) \quad \text{with} \quad c_{\mathrm{F}} \geq 0 \tag{32}$$

For an extended discussion of phase change in this context, see [20].

4 Governing Equations and Numerical Implementation

Free energy formulations for the finite-strain setting can be found in [14, 10, 20] and others. Based on the general constitutive setting outlined above, considerations are now limited to the small strain setting using the decomposition in Eq. (7). For an initial implementation with the purpose of algorithmic testing, some of the physical terms occurring as a consequence of the above derivations and the chosen energy functionals have been neglected. They will be added subject to their relevance indicated by an order-of-magnitude analysis. The following set of governing equations has been implemented into OpenGeoSys [21] for initial testing.

Mixture volume balance

$$0 = \operatorname{div}\left[(\mathbf{u}_\mathrm{S})'_\mathrm{S} + \phi_\mathrm{L}\mathbf{w}_\mathrm{LS}\right] + \hat{\varrho}_\mathrm{I}\left(\varrho_\mathrm{LR}^{-1} - \varrho_\mathrm{IR}^{-1}\right) - \beta_T T'_\mathrm{S} \quad \text{with} \quad \beta_T = \sum_\alpha \phi_\alpha \beta_{T\alpha} \tag{33}$$

Mixture momentum balance

$$\begin{aligned}\operatorname{div}\,(-p_\mathrm{LR}\mathbf{I} + \lambda_\mathrm{S}\mathrm{tr}(\boldsymbol{\epsilon}_\mathrm{S})\mathbf{I} + 2\mu_\mathrm{S}\boldsymbol{\epsilon}_\mathrm{S} - 3\alpha_{T\mathrm{S}}k_\mathrm{S}(T - T_{\mathrm{S}0})\mathbf{I} + \lambda_\mathrm{I}\mathrm{tr}(\boldsymbol{\epsilon}_\mathrm{I})\mathbf{I} + 2\mu_\mathrm{I}\boldsymbol{\epsilon}_\mathrm{I} - \\ 3\alpha_{T\mathrm{I}}k_\mathrm{I}(T - T_{\mathrm{I}0})\mathbf{I} - 3\alpha_{\mathrm{FI}}k_\mathrm{I}(\phi_\mathrm{I} - \phi_{\mathrm{I}0})\mathbf{I}) + \varrho\mathbf{b} = \mathbf{0}\end{aligned} \tag{34}$$

Mixture energy balance

$$(\varrho c_p)^{\mathrm{eff}} T'_\mathrm{S} - \Delta H_\mathrm{I}\hat{\varrho}_\mathrm{I} - \operatorname{div}(\lambda_{\mathrm{SIL}}\operatorname{grad} T) + \varrho_{\mathrm{LR}} c_{p\mathrm{L}}\phi_\mathrm{L}\mathbf{w}_{\mathrm{LS}}\cdot\operatorname{grad} T = 0 \tag{35}$$

The corresponding weak forms are linearized using a Newton-Raphson scheme. The discretized primary variable field $\mathbf{u}_\mathrm{S}$ is interpolated with shape functions an order higher than those used for the remaining primary variables p_LR and T.

5 Verification

Due to the complexity of the fully coupled thermo-hydro-mechanical freezing process and the associated lack of analytical solutions, the initial verification is here separated into a pure thermo-hydro-mechanical part and a pure phase change part, both using analytical solutions.

5.1 Verification of the THM model

In this benchmark, phase change is neglected and a completely sealed specimen is heated up homogeneously. The difference of the thermal expansion coefficients of fluid and solid phase results in a pore pressure which can be determined analytically in the case of an elastic solid skeleton [22]:

$$p_\mathrm{LR} = -K_\mathrm{S}\phi_\mathrm{F}(\beta_{T\mathrm{F}} - \beta_{T\mathrm{S}})\Delta T \tag{36}$$

where K_S is the bulk modulus of the solid matrix, ϕ_F is the porosity and $\beta_{T\mathrm{S}}$= 2.1e-5 and $\beta_{T\mathrm{F}}$ =2.07e-4 are the volumetric thermal expansion coefficients of solid and fluid. Under a homogeneous temperature increment of 80 K, a fluid pressure of 0.1042 MPa develops in the

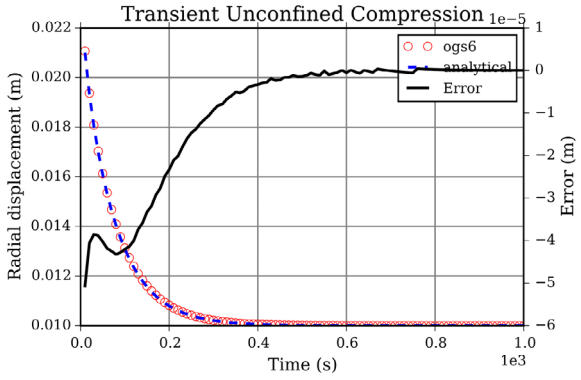

(a) Radial displacement during unconfined compression.

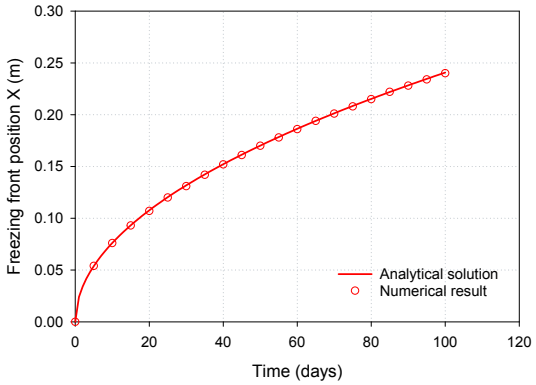

(b) The propagation of the freezing front X over time.

externally load-free specimen under undrained conditions. This value is recovered by the numerical model with a relative error below 10^{-6}. Numerically, the direct linear solver SparseLU (`http://eigen.tuxfamily.org`) and nonlinear tolerances 10^{-8} (absolute error) have been used.

Other tests performed for verification of the THM coupling included transient confined and unconfined compression tests (Fig. 1a) as well as flow under thermal gradients; further details can be found in `https://dev.opengeosys.org/docs/benchmarks/`.

5.2 Phase change verification

In this benchmark, only the thermal problem including phase change is considered and the propagation of the freezing front is calculated by the Neumann analytical solution [23]. A 1 m long water column (achieved by setting the porosity to unity) was connected to a freezing wall of -3 °C. The initial temperature was given as 2 °C in the entire domain. All parameters used in the simulation can be found in [5]. The location of the phase change front $X(t)$ is compared to the analytical solution in Fig. 1b.

6 Numerical Example

In this section, an academic example of the thermo-hydro-mechanical freezing model uses an axisymmetric setup of a cylinder with a radius and height of side 1.0 cm. The domain is divided into 100 elements and the simulation time of 1000 s is split into time steps of 50 s. The externally load-free specimen has an initial temperature of 5 °C. At the bottom, a constant temperature of -5 °C is set as boundary condition. In Fig. 1, the evolving ice saturation with the associated expansion of the specimen is depicted.

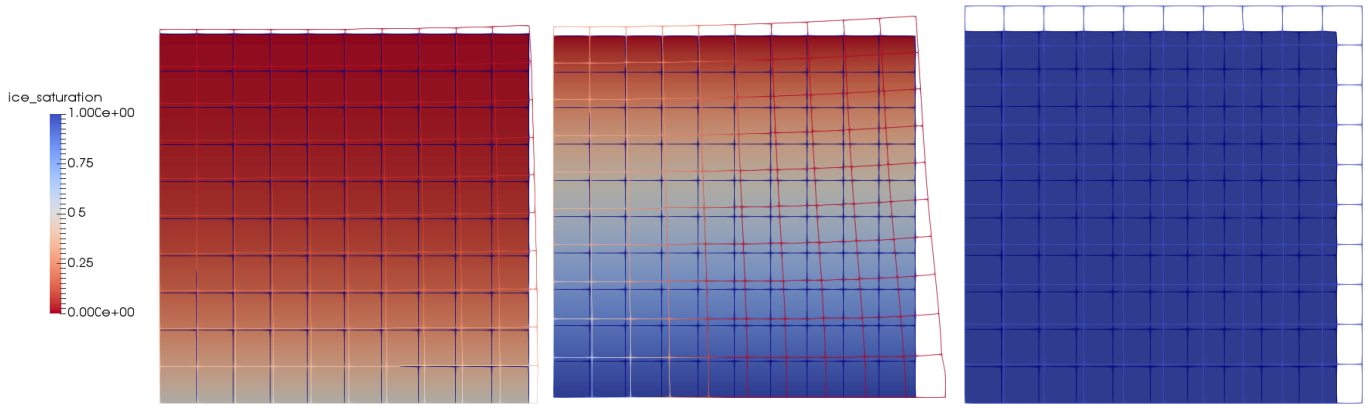

(a) 50 s (b) 150 s (c) 1000 s

Figure 1: Freezing front evolution (colors) and displacement field (overlay grid) during freezing propagation.

7 Conclusion

In this paper, a macroscopic fully coupled thermo-hydro-mechanical model under the framework of the Theory of Porous Media is presented for the simulation of liquid-solid phase change considering effects like the ice volume expansion, hydraulic pressure changes, and the latent effect. It is verified separately with different transient analytical solutions and will be further used to predict the frost evolution around bore-hole heat exchangers.

References

[1] Q. Jilin, Z. Jianming, Z. Yuanlin, Influence of freezing-thawing on soil structure and its soil mechanics significance, Chinese Journal of Rock Mechanics and Engineering 22 (2) (2003) 690–2.

[2] M. Zhou, G. Meschke, A three-phase thermo-hydro-mechanical finite element model for freezing soils, International Journal for Numerical and Analytical Methods in Geomechanics 37 (18) (2013) 3173–3193.

[3] A. Kabuth, A. Dahmke, C. Beyer, L. Bilke, F. Dethlefsen, P. Dietrich, R. Duttmann, M. Ebert, V. Feeser, U.-J. Görke, R. Köber, W. Rabbel, T. Schanz, D. Schäfer, H. Würdemann, S. Bauer, Energy storage in the geological subsurface: dimensioning, risk analysis and spatial planning: the angus+ project, Environmental Earth Sciences 76 (1) (2016) 23. doi:10.1007/s12665-016-6319-5.

[4] S. Erol, B. François, Freeze damage of grouting materials for borehole heat exchanger: Experimental and analytical evaluations, Geomechanics for Energy and the Environment 5 (2016) 29–41.

[5] T. Zheng, H. Shao, S. Schelenz, P. Hein, T. Vienken, Z. Pang, O. Kolditz, T. Nagel, Efficiency and economic analysis of utilizing latent heat from groundwater freezing in the context of borehole heat exchanger coupled ground source heat pump systems, Applied Thermal Engineering 105 (2016) 314–326.

[6] H. Esen, M. Inalli, Y. Esen, Temperature distributions in boreholes of a vertical ground-coupled heat pump system, Renewable Energy 34 (12) (2009) 2672–2679.

[7] W. Yang, L. Kong, Y. Chen, Numerical evaluation on the effects of soil freezing on underground temperature variations of soil around ground heat exchangers, Applied Thermal Engineering 75 (2015) 259–269.

[8] Y. Wang, Q. Gao, X. Zhu, M. Yu, X. Zhao, Experimental study on interaction between soil and ground heat exchange pipe at low temperature, Applied Thermal Engineering 60 (1) (2013) 137–144.

[9] W. Ehlers, Foundations of multiphasic and porous materials, in: W. Ehlers, J. Bluhm (Eds.), Porous Media: Theory, Experiments and Numerical Applications, Springer, Berlin, 2002, pp. 4–86.

[10] J. Bluhm, T. Ricken, M. Bloßfeld, Ice Formation in Porous Media, in: B. Markert (Ed.), Advances in Extended and Multifield Theories for Continua, Vol. 59 of Lecture Notes in Applied and Computational Mechanics, Springer Berlin Heidelberg, 2011, pp. 153–174. doi:10.1007/978-3-642-22738-7_8.

[11] R. de Boer, Thermodynamics of Phase Transitions in Porous Media, Applied Mechanics Reviews 48 (10) (1995) 613–622. doi:10.1115/1.3005042.

[12] M. Mikkola, J. Hartikainen, Mathematical model of soil freezing and its numerical implementation, International Journal for Numerical Methods in Engineering 52 (5-6) (2001) 543–557.

[13] O. Coussy, Poromechanics of freezing materials, Journal of the Mechanics and Physics of Solids 53 (8) (2005) 1689–1718.

[14] J. Bluhm, T. Ricken, W. M. Bloßfeld, Energetische aspekte zum gefrierverhalten von wasser in porösen strukturen, PAMM 8 (1) (2008) 10483–10484. doi:10.1002/pamm.200810483.

[15] N. Li, F. Chen, B. Xu, G. Swoboda, Theoretical modeling framework for an unsaturated freezing soil, Cold Regions Science and Technology 54 (1) (2008) 19–35.

[16] N. Li, F. Chen, B. Su, G. Cheng, Theoretical frame of the saturated freezing soil, Cold Regions Science and Technology 35 (2) (2002) 73–80.

[17] Z. Liu, X. Yu, Coupled thermo-hydro-mechanical model for porous materials under frost action: theory and implementation, Acta Geotechnica 6 (2) (2011) 51–65.

[18] Y. Lai, W. Pei, M. Zhang, J. Zhou, Study on theory model of hydro-thermal–mechanical interaction process in saturated freezing silty soil, International Journal of Heat and Mass Transfer 78 (2014) 805–819.

[19] C. Truesdell, W. Noll, The Non-Linear Field Theories of Mechanics, in: S. Antman (Ed.), The Non-Linear Field Theories of Mechanics, Springer Berlin Heidelberg, 2004, pp. 1–579. doi:10.1007/978-3-662-10388-3_1.

[20] W. Ehlers, K. Häberle, Interfacial mass transfer during gas–liquid phase change in deformable porous media with heat transfer, Transport in Porous Media 114 (2) (2016) 525–556.

[21] O. Kolditz, S. Bauer, L. Bilke, N. Böttcher, J. O. Delfs, T. Fischer, U. J. Görke, T. Kalbacher, G. Kosakowski, C. I. McDermott, C. H. Park, F. Radu, K. Rink, H. Shao, H. B. Shao, F. Sun, Y. Y. Sun, A. K. Singh, J. Taron, M. Walther, W. Wang, N. Watanabe, Y. Wu, M. Xie, W. Xu, B. Zehner, Opengeosys: an open-source initiative for numerical simulation of thermo-hydro-mechanical/chemical (thm/c) processes in porous media, Environmental Earth Sciences 67 (2) (2012) 589. doi:10.1007/s12665-012-1546-x.

[22] X.-Y. Miao, C. Beyer, U.-J. Görke, O. Kolditz, H. Hailemariam, T. Nagel, Thermo-hydro-mechanical analysis of cement-based sensible heat stores for domestic applications, Environmental Earth Sciences 75 (18) (2016) 1293.

[23] J. M. McKenzie, C. I. Voss, D. I. Siegel, Groundwater flow with energy transport and water–ice phase change: numerical simulations, benchmarks, and application to freezing in peat bogs, Advances in water resources 30 (4) (2007) 966–983.